Flow of supersonic jets across flat plates: Implications for ground-level flow from volcanic blasts

Mara M. Orescanin[1,2], David Prisco[3], Joanna M. Austin[4], and Susan W. Kieffer[1]

[1]Department of Geology, University of Illinois, Urbana, Illinois, USA, [2]Department of Mechanical Engineering, Massachusetts Institute of Technology, Cambridge, Massachusetts, USA, [3]Department of Mechanical Sciences and Engineering, University of Illinois, Urbana, Illinois, USA, [4]Department of Aerospace Engineering, University of Illinois, Urbana, Illinois, USA

Abstract We report on laboratory experiments examining the interaction of a jet from an overpressurized reservoir with a canonical ground surface to simulate lateral blasts at volcanoes such as the 1980 blast at Mount St. Helens. These benchmark experiments test the application of supersonic jet models to simulate the flow of volcanic jets over a lateral topography. The internal shock structure of the free jet is modified such that the Mach disk shock is elevated above the surface. In elevation view, the width of the shock is reduced in comparison with a free jet, while in map view the dimensions are comparable. The distance of the Mach disk shock from the vent is in good agreement with free jet data and can be predicted with existing theory. The internal shock structures can interact with and penetrate the boundary layer. In the shock-boundary layer interaction, an oblique shock foot is present in the schlieren images and a distinctive ground signature is evident in surface measurements. The location of the oblique shock foot and the surface demarcation are closely correlated with the Mach disk shock location during reservoir depletion, and therefore, estimates of a ground signature in a zone devastated by a blast can be based on the calculated shock location from free jet theory. These experiments, combined with scaling arguments, suggest that the imprint of the Mach disk shock on the ground should be within the range of 4–9 km at Mount St. Helens depending on assumed reservoir pressure and vent dimensions.

1. Introduction: Geologic and Fluid Dynamic Background

Laterally directed gas and debris flows can be produced either by collapse of a sector of a volcano or by collapse of a column that was initially vertically directed. Such flows travel nearly parallel to, and interact with, ground surfaces. These damaging flows can reach velocities of greater than 100 m/s [*Moore and Rice*, 1984; *Hoblitt*, 2000] and can be internally supersonic for distances of kilometers, depending on the vent geometry and pressure of the magma chamber [*Kieffer*, 1981, 1982]. The lateral blast at Mount St. Helens on 18 May 1980 discharged across downward sloping flanks of the volcano for about 7 km, crossed the North Fork Toutle River, and then climbed up into high country. The velocity of the front was nearly constant at 100 m/s for much of this distance [*Moore and Rice*, 1984], an observation that suggests that accelerations and decelerations of gravity had no net effect over roughly the first 10 km of travel.

Based on this observation and estimates that the pressure ratio between the magma chamber and ambient atmosphere was roughly 150:1, *Kieffer* [1981, 1982] proposed that the lateral blast resembled the discharge of a large supersonic rocket nozzle pointed laterally toward the north and estimated the nature of internal shock structures from experiments on free jets discharging into an atmosphere. She proposed that a Mach disk shock existed in the flow at a distance of 11 km from the vent, later revising this to about 5.7–9 km using an updated model for vent dimensions and a wider range of pressure ratios [*Orescanin et al.*, 2010]. Subsequently, the existence of the supersonic shock structures and the distance from the vent at which they might occur have been challenged based on multiphase computational simulations [*Esposti Ongaro et al.*, 2011, 2012]. In this paper, we report the results of 3-D laboratory experiments designed to investigate the interaction of free supersonic jets with a ground layer and apply the results to the controversy described above.

Theories of free jets have been applied to vertically directed eruptions, for example, Plinian eruptions [*Ogden et al.*, 2008a, 2008b; *Ogden*, 2011], and to lateral blasts [*Kieffer*, 1981, 1982; *Orescanin et al.*, 2010] to model the global flow field. The effect of topography on the structure of a jet has been investigated

computationally at a coarse scale starting with studies in the 1980s and 1990s such as *Valentine et al.* [1992], and more recently with higher resolution, but still relatively coarse grids by *Esposti Ongaro et al.* [2008, 2011, 2012].

To include three dimensions, to apply to geographical areas that may be hundreds of square kilometers, to incorporate multiple particle sizes, and to make the codes computationally feasible, spatial resolution must be sacrificed. This creates two potential problems. First, shock waves which can occur in supersonic flow can be smeared due to numerical dissipation unless special techniques are used. Second, boundary layers can be difficult to resolve adequately. Field relations at Mount St. Helens suggest that at a distance of about 8 km, the boundary layer was 14 m thick [*Kieffer and Sturtevant*, 1984], a result that is reasonable agreement with boundary layer thicknesses from two independent models. The first is the "law of the wake" combined with the "momentum integral relation" for the growth of turbulent boundary layers based on experiments over flat plates. The second is the Blasius equation from experiments on turbulent pipe flow. These two relations yield distances for a 14 m thick boundary layer of 4.2 and 10.3 km, respectively. In contrast, boundary layers in the numerical codes are predicted to be hundreds of meters thick [e.g., see *Esposti Ongaro et al.*, 2007, 2012]. *Esposti Ongaro et al.* [2007] had stated that at least five cells are required to describe accurately a boundary layer in multiphase flow. In the best codes, cell sizes are 10 m or more in vertical dimension leading to boundary layers predicted to be hundreds of meters thick [e.g., *Esposti Ongaro et al.*, 2007, 2012]. Therefore, in addition to the smearing out of shock waves due to numerical dissipation, grid sizes required for computational feasibility may be overestimating the size of boundary layers.
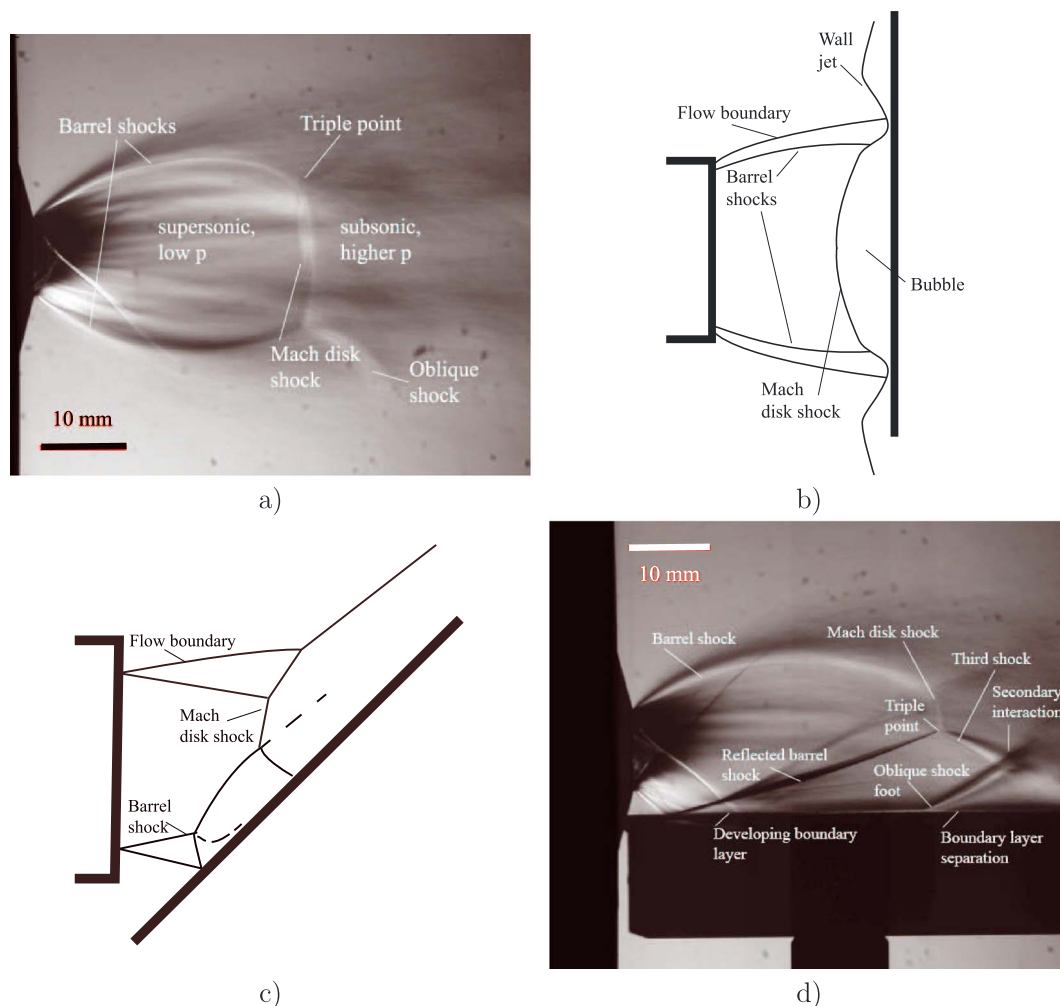
Given the difficulty of benchmarking codes against field evidence, we argue that all codes using pure gases or gas mixtures should be compared with laboratory experiments also in gases without particles because particles will smear out the effects and cannot easily be scaled to the laboratory. The behavior of particles can then be included in computer codes with appropriate forces acting on them, but only if the fundamental gas behavior is modeled correctly. Noting the good agreement between 3-D free jet experiments and 1-D models, *Ogden et al.* [2008a] were able to benchmark their simulations based on Mach disk shock standoff distance. A discrepancy in the vertical velocity and plume radius due to limitations of 1-D models was noted. Recently, *Carcano et al.* [2013] extended the existing code used by *Esposti Ongaro et al.* [2012] to achieve higher accuracy and robustness in the resolution of compressible regimes, while reducing the numerical diffusion. Simulations using the higher-order numerics were compared with free jet data and simulations. To date, there have been few three-dimensional laboratory simulations appropriate for benchmarking the numerical codes. In this study, we provide a simple data set that can be used for this purpose: a supersonic jet flowing over a plate parallel to its flow direction, simulating the flow of a volcanic jet over a flat smooth terrain. Jet impingement onto a surface has been studied extensively in normal [*Donaldson and Snedeker*, 1971; *Carling and Hunt*, 1974; *Lamont and Hunt*, 1980; *Lengrand et al.*, 1982] and oblique orientations [*Lamont and Hunt*, 1980; *Wu et al.*, 2002; *Nakai et al.*, 2006; *Crafton et al.*, 2006]. To the authors' knowledge, previous investigations of jet impingement on parallel plates are limited to acoustic studies [*Wlezien*, 1989] or high-vacuum systems [*Ivanov and Nazarov*, 1974].

2. Jet Structures

An unconfined overpressured jet contains a supersonic core bounded by *barrel shocks*, a normal shock referred to as a *Mach disk shock*, and *oblique shocks* (Figure 1a). High-speed flow decelerates through all shocks. For an unconfined, underexpanded jet, the normalized location of the Mach disk shock is primarily a function of the reservoir-to-ambient pressure ratio and secondarily of the ratio of specific heats [*Ashkenas and Sherman*, 1966; *Crist et al.*, 1966].

Impingement on a plate normal to the flow (Figure 1b) increases the stagnation pressure downstream of the Mach disk shock [*Donaldson and Snedeker*, 1971; *Carling and Hunt*, 1974; *Lamont and Hunt*, 1980; *Lengrand et al.*, 1982]. Because of this effect, the Mach disk shock standoff distance decreases with decreasing separation distance between the plate and jet exit [*Khalil and Miller*, 2004]. In normal impingement, an outflow parallel to the wall develops, a so-called *wall jet*, which contains a series of compression and expansion waves [*Lamont and Hunt*, 1980] (Figure 1b). The maximum pressure across the impingement region occurs in the center of the flow and pressure distribution decays radially from this maximum [*Donaldson and Snedeker*, 1971; *Carling and Hunt*, 1974; *Lamont and Hunt*, 1980; *Lengrand et al.*, 1982].

Impingement on an inclined plate shifts the location of maximum pressure and of the stagnation point, as a function of the downstream distance (Figure 1c) [*Lamont and Hunt*, 1980; *Wu et al.*, 2002; *Nakai et al.*, 2006;

Figure 1. Underexpanded jet structures for (a) a free jet and a jet impinging on a (b) perpendicular, (c) inclined, and (d) parallel surfaces. Figure 1b is after *Lamont and Hunt* [1980]. Figure 1c is after *Plemmons et al.* [2008]. Figures 1a and 1d are schlieren images obtained at pressure ratios of 23 and 32, respectively.
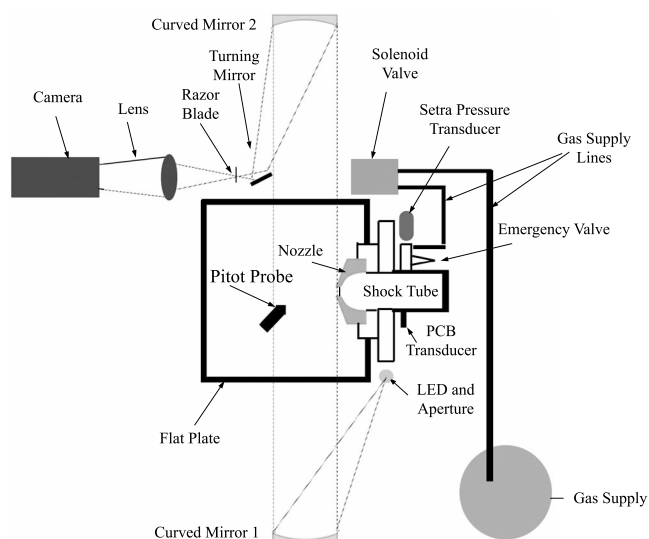
Crafton et al., 2006]. *Lamont and Hunt* [1980] find that the maximum pressure is substantially larger for an inclined plate than for a normal plate for a given downstream distance. These results were confirmed by *Crafton et al.* [2006], who experimentally measured the surface pressure and jet velocity associated with jet impingement on an inclined plate with pressure sensitive paint and particle image velocimetry.

To briefly complete the discussion of terminology and introduce our results, we show the structure of one of our laboratory jets parallel to the wall in Figure 1d. The Mach disk shock is disconnected from the surface, as in the case of the inclined plate (Figure 1c). Almost directly below the Mach disk shock location, a *shock wave–boundary layer interaction* results in an *oblique shock foot* that impinges on the plate. Pressure gradients across shock waves interact with the flow along the surface causing upstream thickening of the boundary layer, external flow compression via the oblique shock, and *flow (boundary layer) separation* on the surface downstream of the oblique shock foot.

We first investigate whether the presence of the parallel surface will change the features of the jet, in particular the location of the Mach disk shock that separates supersonic and subsonic flows. Secondly, we examine the ground signature resulting from the interaction of the jet with the surface and the implications for devastation due to a lateral blast, such as occurred at Mount St. Helens.

3. Laboratory Setup

Experiments were conducted in an open-ended shock tube facility (Figure 2). The shock tube consisted of a cylindrical reservoir with 50 mm inner diameter and 50 mm length attached to a convergent nozzle
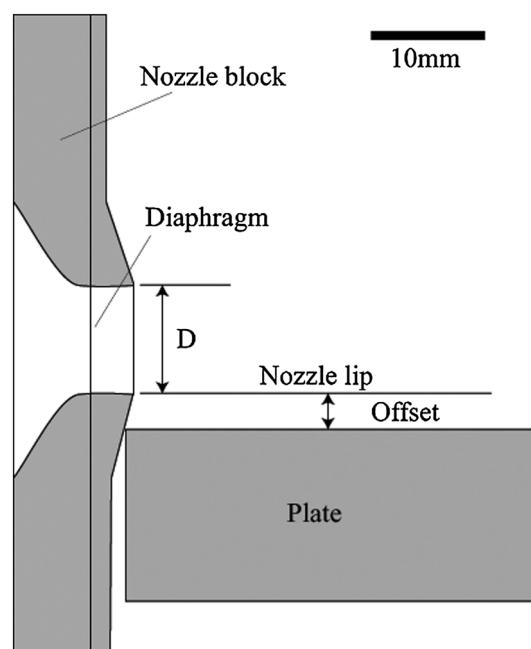
Figure 2. Schematic of experimental setup (not to scale).

(Figure 3). Near the exit of the nozzle, or vent, a Mylar diaphragm initially separated the high-pressure nitrogen gas in the reservoir from the ambient air. The initial reservoir to ambient pressure ratio varied from approximately 30:1 to 40:1 for all experiments discussed here. The initial reservoir pressures for each experiment are included in Table 1. More details on the experimental facility can be found in *Orescanin et al.* [2010].

The experiment initiated with the rupture of the diaphragm. The depleting reservoir pressure ratio is measured using a piezoelectric gauge with 1 μs resolution. The underexpanded jet exhausting from the reservoir propagated over an optically transparent flat plate mounted either vertically or horizontally relative to the imaging plane (Figure 2). The jet was visualized using a single-shot schlieren technique, as described in *Orescanin et al.* [2010], as it propagated across the plate in two views: (i) from the side, corresponding to a elevation view, or (ii) from above the plate, corresponding to a map view. In the latter case, the images were backlit through the transparent plate. The resolution of measurements made from schlieren images was 0.25 mm. The vertical distance of the plate from the lip of the nozzle was varied from 0 mm, i.e., in direct contact, to 3 mm, that is from 0D to 0.3D where D = 10 mm is the diameter of the nozzle. The purpose of choosing these two configurations was to simulate both a volcanic jet that travels along the ground immediately upon exiting a vent (0D) versus one that first travels some distance above the ground (e.g., across a valley) before hugging the ground

Figure 3. Detail of the shock tube nozzle and plate for a 3 mm (0.3D) offset. The nozzle has a throat diameter D of 10 mm. A diaphragm is located 4 mm from the nozzle exit plane. A 50 mm reservoir is connected to the block (outside the field of view).

(0.3D). Data acquisition was triggered by the arrival of the initial shock wave at a dynamic pressure gauge (with 1 μs response time) located in the far field, off axis from the jet exhaust. The gauge signal acquisition was synchronized with the reservoir pressure measurement. A high-speed video (which could be manually triggered) was recorded with and without the gauge present to ensure it had no effect on the jet.

Qualitative surface flow visualizations were also made using pressure sensitive paint (PSP) and shear stress (S3F) paint applied to the plates [*Crafton et al.*, 2011]. A platinum tetra(pentafluorophenyl)porphine-based porous polymer paint manufactured by Innovative Scientific Solutions, Inc. (ISSI) was used. The response time of this PSP was on the order of 30 to 50 μs [*Flaherty et al.*, 2014]. Qualitative measurements were also made using a surface stress sensitive film (S3F) [*Fonov et al.*, 2006]. Markers are applied to a thin film, and the displacement is measured. The two diagnostics were used to ensure the surface signature was not dependent on the measurement

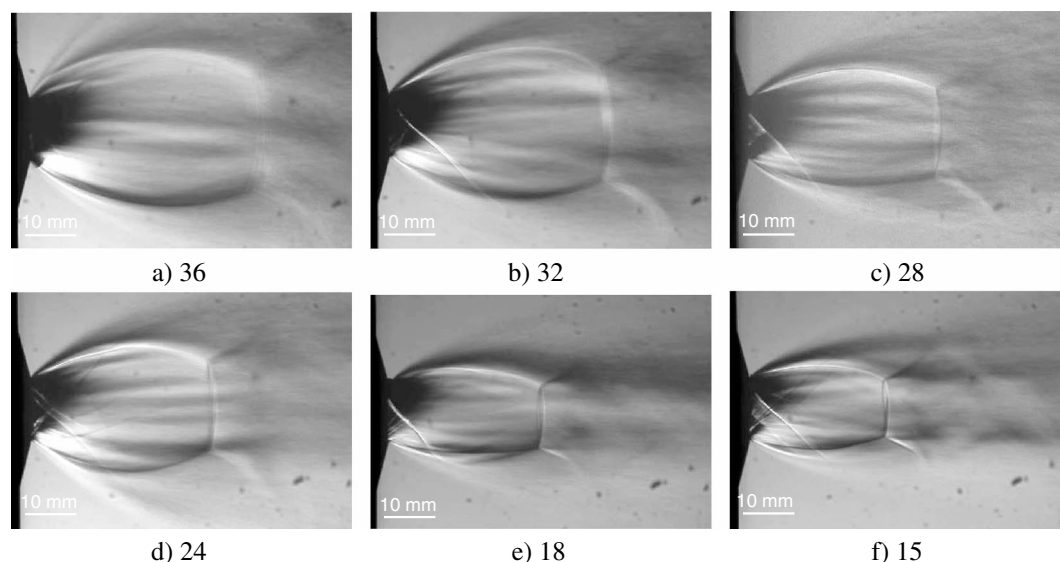**Table 1.** The Experimental Conditions for Each of the Schlieren Images Shown in the Paper[a]

Figure Number	Shot Number	Initial Reservoir Pressure (atm)	Mean Pressure Ratio	Figure Number	Shot Number	Initial Reservoir Pressure (atm)	Mean Pressure Ratio
4a	442	37.5	36	4d	455	41.4	24
4b	443	37.6	32	4e	452	38.8	18
4c	433	37.9	28	4f	457	40.0	15
5a	444	38.6	37	5d	447	41.3	24
5b	445	37.5	32	5e	448	41.3	19
5c	446	41.4	30	5f	449	39.0	15
6a	440	36.3	35	6d	457	40.0	23
6b	441	37.5	32	6e	452	38.8	18
6c	450	38.3	28	6f	453	40.5	16
7a	488	36.3	35	7d	498	37.7	22
7b	489	36.0	31	7e	499	37.7	18
7c	497	38.0	28	7f	500	38.2	15
8a	491	39.8	39	8d	494	38.0	21
8b	492	36.5	31	8e	495	38.0	18
8c	493	41.7	30	8f	496	38.0	15

[a]Mean pressure refers to the average pressure over the image acquisition time.

technique. The model was illuminated using a liquid-cooled ISSI LM2X-400 light-emitting diode, and a Cooke pco1600 CCD camera was used for image acquisition. Surface measurements using both techniques are obtained as the ratio of intensity between wind-on and wind-off (no-flow) conditions.
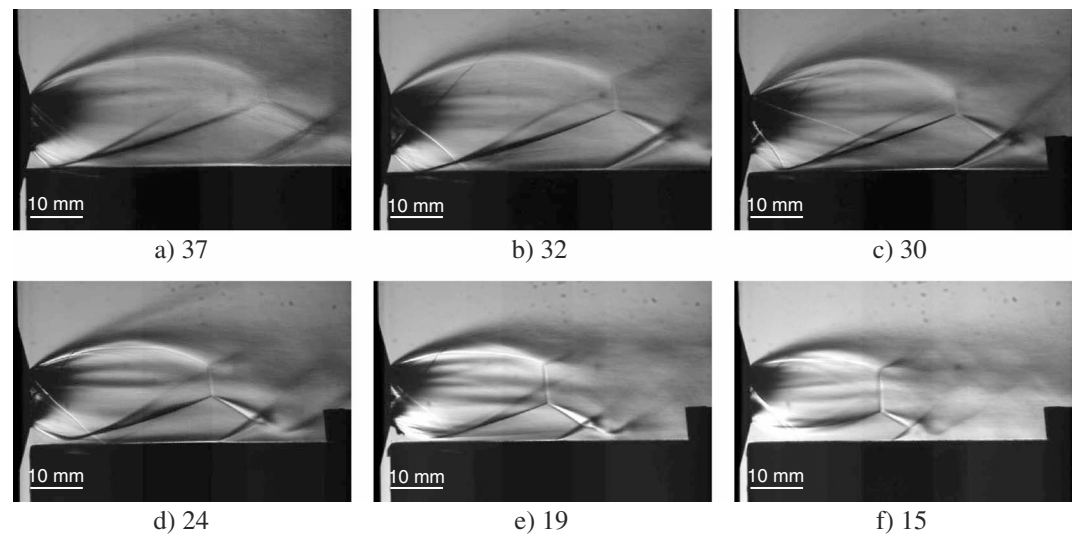
4. Experimental Results

Upon rupture of the diaphragm separating the pressurized reservoir from the ambient air, an underexpanded jet exhausts from the reservoir. Single-shot schlieren images are used to construct a time sequence visualizing the jet structure during the reservoir blowdown. For reference, this "blowdown" of an unconfined jet is first shown in Figure 4. As discussed in section 2, the primary shock structure of the jet consists of two curved barrel shocks, a normal Mach disk shock, and oblique reflected shocks. As the reservoir depletes in time, the shock structure retreats back toward the nozzle vent. Previous work has demonstrated that for reservoir-to-ambient pressure ratios above about 15, the jet structure is self-similar and the Mach disk location can be predicted using steady state empirical relations applied at the instantaneous pressure ratio

a) 36   b) 32   c) 28

d) 24   e) 18   f) 15

Figure 4. Selected series of schlieren images of a free nitrogen jet exhaust during the reservoir blowdown with no plate boundary. Flow is from left to right. Captions indicate the mean reservoir to ambient pressure ratio during image acquisition. Note the migration of the Mach disk toward the nozzle as the reservoir pressure decreases.
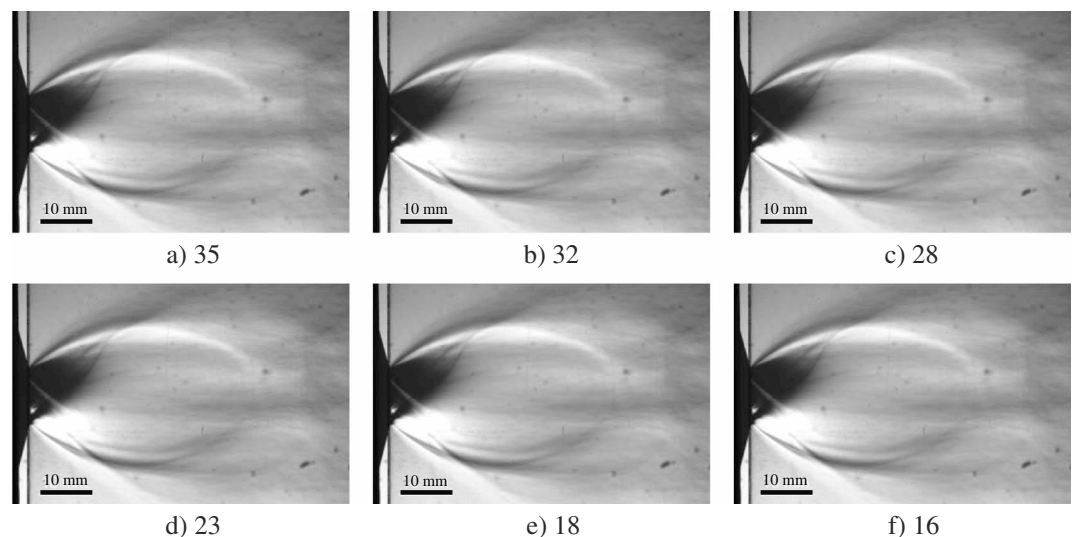
Figure 5. (a–f) Selected series of schlieren images of a nitrogen jet exhaust over a flat plate during the reservoir blow-down (elevation view). Captions indicate the mean reservoir to ambient pressure ratio during image acquisition. The offset of the plate from the vent exit is 3 mm.
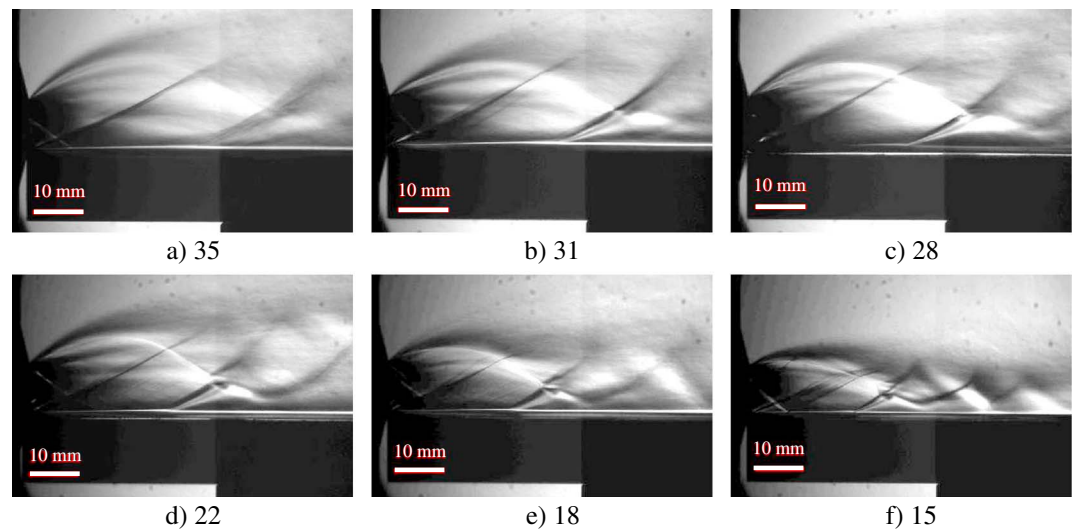
[*Orescanin et al.*, 2010; *Orescanin and Austin*, 2010]. In the experiments reported here, pressure ratios up to 41 are investigated.

In our experiments with a parallel plate, schlieren images of impinging jets are obtained in two planes. Elevation and map views for the 0.3*D* case are shown in Figures 5 and 6, respectively; terminology is identified in Figure 1d. Some features of an unconfined, underexpanded jet can be identified, including the characteristic barrel and Mach disk shocks. However, when the jet impinges on the plate, additional features associated with wave reflections from the plate surface and formation of a boundary layer along the plate arise. The presence of the surface results in the loss of the axisymmetric jet structure and the formation of a complex three-dimensional flow.

In the elevation view of the jet with the plate offset by 0.3*D*, the free jet structure is observed in the top half of the image, including the normal Mach disk shock (Figure 5a). However, due to the surface interaction the Mach disk shock is elevated above the flat plate and its diameter is reduced. The reflection of the
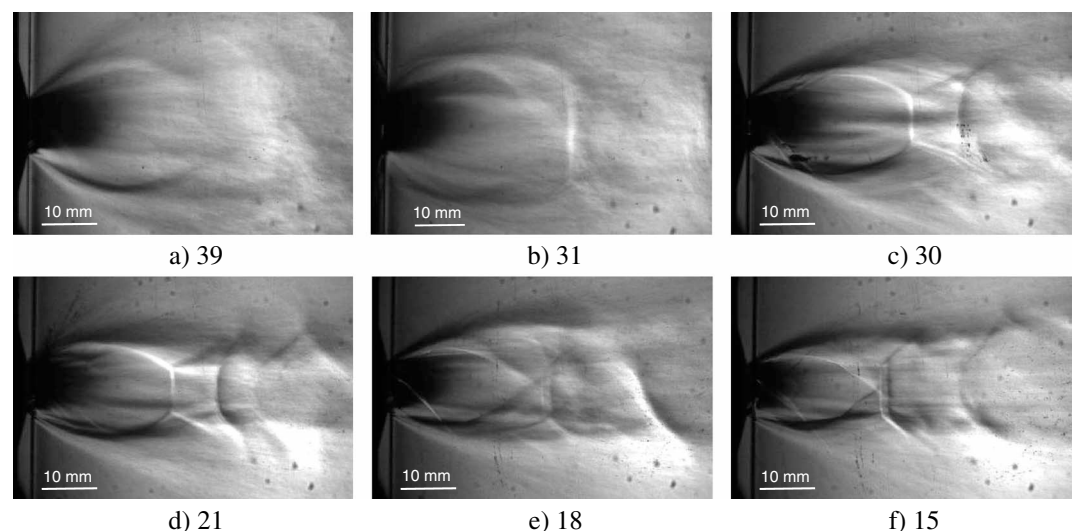

Figure 6. Selected series of schlieren images of a nitrogen jet exhaust over a flat plate during the reservoir blowdown (map view). Captions indicate the mean reservoir to ambient pressure ratio during image acquisition. The offset of the plate from the vent exit is 3 mm.
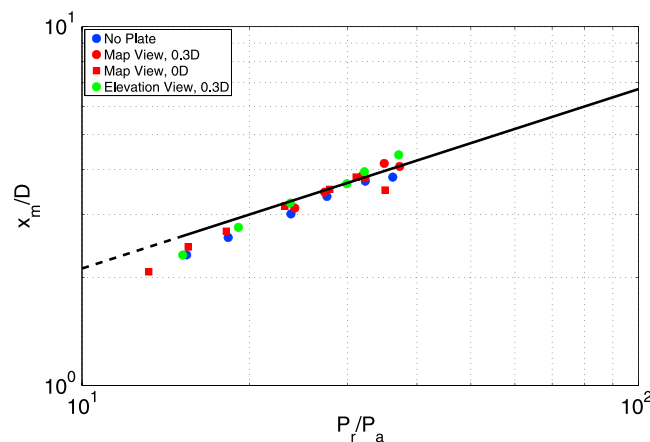
Figure 7. (a–f) Selected series of schlieren images of a nitrogen jet exhaust over a flat plate during the reservoir blow-down (elevation view). Captions indicate the mean reservoir to ambient pressure ratio during image acquisition. The plate is positioned directly at the vent lip (0 mm offset). Data are corrected for variations in the pitot probe location (seen on Figures 7a and 7d).

barrel shock from the plate is observed near the vent. The reflected barrel shock intersects the Mach disk shock at a (three-shock) triple point. The third shock emanating from the triple point is directed back toward the plate along which a boundary layer is developing. The interaction of pressure gradients with the boundary layer causes the upstream boundary layer to thicken and the flow potentially to separate [*Mark*, 1958; *Liepmann and Roshko*, 2001]. The compression of the flow in the region of boundary layer thickening results in an oblique shock wave and apparent separation region. Importantly for our results, the foot of the oblique shock is located almost directly below the Mach disk shock location for all pressure ratios. As a result, the oblique shock foot cannot always be distinguished from the Mach disk shock in the map view of the jet due to the integrating nature of the schlieren visualization (Figure 6). Additional shocks, most noticeably secondary (Figure 1d) and even tertiary interactions, are evident downstream.

Figure 8. (a–f) Selected series of schlieren images of a nitrogen jet exhaust over a flat plate during the reservoir blow-down (map view). Captions indicate the mean reservoir to ambient pressure ratio during image acquisition. The plate is positioned directly at the vent lip (0 mm offset). Data are corrected for variations in the pitot probe location (seen on Figures 8a and 8d).

Figure 9. Mach disk standoff distance versus instantaneous pressure ratio. The black solid line is the empirical relation of *Ashkenas and Sherman* [1966] (equation (1)). Dashed line corresponds to an extrapolation of the fit below a pressure ratio of 15.

Images of the jet structure interacting with a plate emanating directly from the lip of the nozzle (offset = 0D) are shown in Figures 7 (elevation view) and 8 (map view). There are several observable differences between the cases with 0D and 0.3D offsets. In the elevation view of the 0D case, the reflection of the barrel shock occurs at the nozzle, and from this point downstream the axial symmetry is destroyed. A distinct Mach disk shock is not evident in this view. In the map view, however, a normal shock is evident between the barrel shocks (Figure 8, denoted "map view shock feature"). By comparing the map and elevation views, we see that the ground is again marked by the oblique shock associated with the shock-boundary layer interaction.

5. Discussion

5.1. Effect of Jet Impingement on a Parallel Surface

For a free jet exhausting from a finite reservoir with continuously decreasing reservoir pressure, our previous studies have shown that the Mach disk shock location can be predicted using the steady state correlation evaluated at the instantaneous pressure, above pressure ratios of about 12:1 to 15:1 [*Orescanin et al.*, 2010; *Orescanin and Austin*, 2010]. Therefore, the location of the Mach disk shock can be predicted by the *Ashkenas and Sherman* [1966] relation:

$$\frac{x_m}{D} = 0.67 \left(\frac{P_r}{P_a} \right)^{\frac{1}{2}} \tag{1}$$

where x_m is the standoff distance of the Mach disk shock, P_r is the instantaneous reservoir pressure, and P_a is the instantaneous ambient pressure.
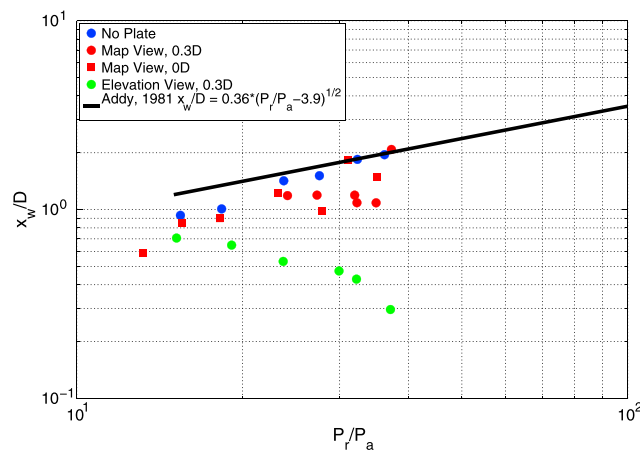
For a given experiment, we measured the lateral distance from the vent exit to the Mach disk shock from each schlieren image. The images were obtained at selected times during the blowdown of the reservoir by setting a delay to the camera acquisition. The reservoir pressure was recorded for each experiment as a function of time. The reservoir pressure value corresponding to the image acquisition could therefore be determined (Table 1). The normalized results are shown in Figure 9. In the region where the free jet correlation applies, both map and elevation views for both 0D and 0.3D offsets indicate that the Mach disk shock location is well predicted by the free jet correlation of *Ashkenas and Sherman* [1966] (equation (1)), if evaluated at the instantaneous pressure ratio.

The decrease in the vertical extent (width and height above the plate) of the Mach disk shock due to the interaction with the plate is evident in the schlieren images and in a comparison of measurements of the width of the shock in map and elevation views respectively with the width in a free jet (Figure 10). Note that no distinct Mach disk shock is evident in the 0D map view, and therefore, no data are presented. In the 0.3D map view, the Mach disk shock and oblique shock foot are coincident to within the resolution of the experiments; thus, the width of the map view normal shock feature (Figure 8c) is measured and reported here.

Addy [1981] observed that the diameter of the Mach disk shock is proportional to the square root of the pressure ratio, based on their free jet experiments. Our free jet data at pressure ratios above about 20 are in reasonable agreement with their correlation, which is consistent with the self-similarity in jet structure (Mach disk shock width to barrel shock width) that has been reported for pressure ratios above about 15 [*Orescanin and Austin*, 2010, Figure 14]. The data are more scattered for the jet with the parallel plate; however, in spite of the scatter, it is clear that the Mach disk has a very different shape in the two cases. In a free

Figure 10. Width of shock feature versus instantaneous pressure ratio. In the elevation view, the Mach disk shock width is measured. In the map view, the width of the map view shock feature (Figure 8c) is measured. A fit (solid line) for the normalized Mach disk shock diameter from *Addy* [1981] is in reasonable agreement with the present free jet data for pressure ratios above about 20. Self-similarity in jet structure has been reported for pressure ratios above about 15 [*Orescanin and Austin*, 2010]. The presence of the plate decreases the width of shock from that of the free jet.

jet, the flow is axisymmetric and the shock width is the same in map and elevation views; that is, it is circular in cross section. When the parallel plate is introduced, the width in map view is about the same, but in the elevation view it is greatly reduced; that is, it becomes closer to ellipsoidal in the ratio of major axes. The width of the Mach disk shock in elevation view decreases slightly with increasing pressure ratio. In contrast, the width of the map view shock feature and of the Mach disk shock in a free jet increase with increasing pressure ratio.

5.2. Shock-Boundary Layer Interaction

As discussed in section 2, shock interaction with the boundary layer can produce a separation region where the flow detaches from the surface.

The separation region is downstream of an oblique shock foot which is evident in the schlieren images. In addition to schlieren visualization, qualitative surface measurements were made using pressure sensitive paint (PSP), shown in Figure 11. The resulting distinctive ground signature associated with shock impingement can be observed clearly as a sudden increase in pressure (denoted "A" in the figure). The spanwise width of the separated region is comparable to the width of the Mach disk shock in the map view.

In the schlieren images, the oblique shock foot impinges the plate at approximately the same horizontal distance from the vent as the (elevated) Mach disk shock (Figure 12a). The measured location of the surface demarcation in the paint measurements and the oblique shock impingement location identified in the schlieren images correspond throughout the blowdown of the reservoir (Figure 12b).
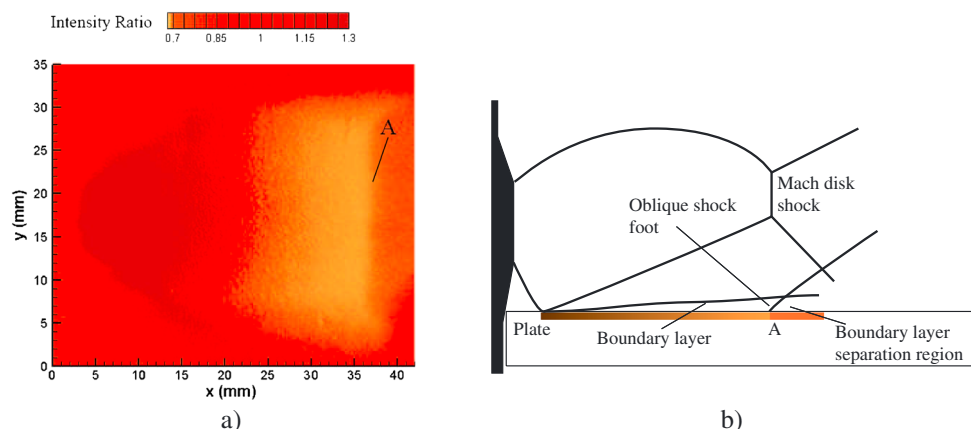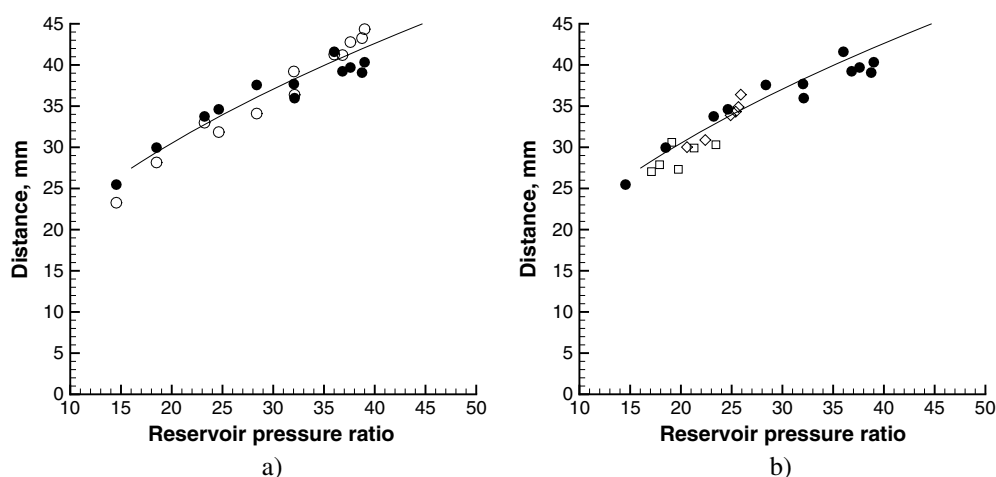
5.3. Implications for Lateral Blasts

Perhaps the most significant result of these laboratory experiments is the fact that structures in the free jet are transmitted through the boundary layer onto the solid boundary (ground) surface, as discussed in section 5.2 and shown in Figures 5, 7, and 11. In addition, the downstream location of the Mach disk shock is

Figure 11. (a) Sample PSP image of the flat plate surface during blowdown in a 0.3*D* offset case (instantaneous reservoir to ambient pressure ratio of 26). These data are qualitative; however, the color indicates levels relative to the ambient pressure. The feature associated with oblique shock impingement is denoted A. Flow is left to right. (b) Sketch showing jet flow features in elevation view which were examined for correlation with surface demarcation.

Figure 12. (a) Measured distance of schlieren features from the nozzle vent as a function of the instantaneous reservoir pressure ratio. All jet features retreat toward the vent as the reservoir pressure depletes. The oblique shock impingement location from schlieren images (open circle), indicated in Figure 1d, corresponds closely to the elevated Mach disk shock location, both in experiments (filled circle) and in the predictions of *Ashkenas and Sherman* [1966] (solid line). (b) Measured distance of surface features downstream of the nozzle vent from PSP data (diamond) and S3F data (square). The demarcation of the onset of flow separation from surface paints (diamond and square), indicated as feature A in Figure 11, corresponds closely to the Mach disk shock location from schlieren images (filled circle). The prediction of Mach disk shock location of *Ashkenas and Sherman* [1966] (solid line) is shown for reference.

unchanged from its position in the free jet by the presence of a parallel flat plate. The Mach disk shock is collocated with the oblique shock foot. Unlike the sharp contrast in flow properties across a Mach disk shock in a free jet, the transition zone in the presence of a flat plate is extended by flow separation (Figure 11), which may make such a transition easier to identify in a field situation than if the transition was simply across a small shock wave.

Within the body of the jets above the boundary layer, there are some similarities and some differences with free jets (Figures 4, 6, and 8). Of specific relevance to the field situation would be changes of the jet structure in map view, if these are projected through the boundary layer, as established above; changes in the elevation view would be much more difficult to document in the field, and so we do not discuss them further. In map view, the Mach disk location remains at the same distance as in the free jet case, but the diameter is smaller than in the free jet case (Figures 9 and 10), perhaps indicating a slightly narrowed destruction zone, depending on the actual distance of the underlying boundary.

As discussed in *Kieffer and Sturtevant* [1984], some aspects of laboratory experiments can be scaled to field observations, and some cannot. However, even in the absence of true scaling, laboratory simulations afford an opportunity to consider processes that may not be evident during or after natural events. In the cases studied here, effects of compressibility can be examined, but effects of gravity, which may be important in large-scale natural eruptions, cannot. However, we expect gravity effects to become important primarily after the transition to internally subsonic flow occurs.

5.4. Comparison With Simulations

The flow-field dynamics of a jet exhausting from a pressurized reservoir are tied to the time-dependent depressurization history of the reservoir or blowdown. With proper scaling, blowdown dynamics from the laboratory can be used to interpret near-vent (proximal) conditions for discharge from high-pressure volcanic reservoirs. Here we use this fact to compare and contrast blowdown models of the 1980 lateral blast at Mount St. Helens.

The model of *Kieffer* [1981] for the dynamics of the lateral blast was an early form of a blowdown model based on a free jet emerging from a pressurized reservoir without interfering surfaces, such as the ground. The 1981 model predated supercomputer capacity, and Kieffer made estimates of the position of the shock from the Ashkenas-Sherman steady state relation (equation (1)) using the longest vent dimension for scaling. The vent was assumed to have an east-west width of 1000 m, a north-south thickness of 500 m, and a height of 250 m. The Mach disk shock was calculated to be at 11 km. Using an improved estimate of reservoir

dimensions based on *Donnadieu and Merle* [2001], *Orescanin et al.* [2010] updated the reservoir to have a width of 850 m, thickness of 100 m, and height 1300 m. Using 850 m as the determining vent dimension, the Mach disk shock was calculated to be at 5.7 km for a pressure ratio of 100:1, at 8.2 km for a pressure ratio of 150:1, or at 9 km for a pressure ratio of 250:1. This current study further shows that the distances calculated for the imprint of the Mach disk shock on the ground are not changed from *Orescanin et al.* [2010].

In contrast to our laboratory experiments that had uniform pressure in a simple cylindrical reservoir that is discharged upon rupture of a diaphragm, supercomputer simulations, such as those of *Esposti Ongaro et al.* [2012], use a much more complicated reservoir geometry and initial pressure distribution. In their simulation of the Mount St. Helens blast, the reservoir pressure was taken to be 10 MPa above hydrostatic in a pressurized conical-shaped portion of a hemisphere. Their initial atmospheric pressure is about 0.070–0.075 MPa at the level of the vent. To simplify these initial conditions for this discussion and to facilitate comparison with the earlier models and lab experiments, we estimate that the hydrostatic pressure at the center of mass of the cone that erupts was roughly 3 MPa, so that an average total pressure of 13 MPa is representative, giving the ratio of vent pressure to atmospheric of ~ 175. We take the vent diameter for their simulations to be the diameter of the base of the spherical cap of their cone, approximately 500 m (their Figure 1). For this diameter and pressure ratio, the Ashkenas-Sherman relation gives the distance out to the Mach disk shock as 4.4 km, almost exactly the distance at which the simulated flow suddenly decelerates at the end of the "burst stage" (their Figure 2b). We suggest that the rapid deceleration observed in the simulations at this distance is the Mach disk shock, smeared out by both computational limitations and multiphase particle effects. Other than this suggestion, our results agree with *Esposti Ongaro et al.* [2012] that, for the particular assumptions of their simulation, gas decompression drives the flow and extends out to about 4–5 km, and the flow becomes gravity driven at greater distances.

However, the simulation represents only one pressure ratio and one vent size. We have done calculations for different vent shapes (rectangular and circular), vent diameters (500 to 1000 m), average pressure ratios (100:1 to 250:1), and total erupted volumes (roughly 0.10 to 0.15 km^3). Our analysis suggests that when simulations such as those of Esposti Ongaro are run through the range of parameters covering these instances, the Mach disk location will range from 4 to 9 km.

In order to simulate volcanic directed blasts, we suggest two requirements for the simulation community. The first is benchmarking numerical codes against laboratory experiments that provide data on the depressurization of the reservoir, its effect on the evolving flow field, and the effect of the ground on the flow. The second is a parametric study of the effect of vent dimensions and pressure ratios. Until both types of simulations have been done, it cannot be stated that there are no internal shocks and supersonic features, nor that the role of gas depressurization can be neglected in the start-up conditions for simulations.

6. Conclusions

These results have several implications for volcanology and have a specific application to Mount St. Helens. For an underexpanded jet exhausting from a finite reservoir and impinging on a flat plate oriented parallel to the flow, the Mach disk standoff distance can be predicted from steady state free jet empirical relations evaluated at the instantaneous pressure ratio, just as previously determined for a finite reservoir free jet. This implies that the Mach disk standoff distance for volcanic eruptions directed parallel to the surrounding topography can be estimated from that predicted for the free volcanic jets, described by the *Ashkenas and Sherman* [1966] relation (equation (1)).

While the Mach disk standoff distance is the same for the free and the impinging underexpanded jets, the Mach disk height is not and depends on the interaction of the jet with a parallel flat plate. The size of the Mach disk shock is reduced, and the impinging jet loses symmetry due to the interaction of the barrel shock with the flat plate.

Internal shocks can interact with and penetrate boundary layers. In particular, the oblique shock foot penetrates the boundary layer and marks the ground at a location closely correlated with the Mach disk shock location throughout the reservoir depletion. Thus, we would expect estimates of a supersonic-subsonic transition in a devastation zone on the ground to be fairly accurate even if based on the location of a calculated free jet Mach disk shock location.

References

Addy, A. L. (1981), Effects of axisymmetric sonic nozzle geometry on Mach disk characteristics, *AIAA J.*, *19*(1), 121–122.

Ashkenas, H., and F. S. Sherman (1966), Experimental methods in rarefied gas dynamics, *Tech. Rep. 32-869*, NASA.

Carcano, S., L. Bonaventura, T. E. Ongaro, and A. Neri (2013), A semi-implicit, second-order accurate numerical model for multiphase underexpanded volcanic jets, *Geosci. Model Dev.*, *6*, 1905–1924.

Carling, J. C., and B. L. Hunt (1974), Near wall jet of a normally impinging, uniform, axisymmetric, supersonic jet, *J. Fluid Mech.*, *66*, 159–176.

Crafton, J., C. Carter, G. Elliott, and J. Sullivan (2006), The impingement of sonic and sub-sonic jets onto a flat plate at inclined angles, *Exp. Fluids*, *41*, 699–710.

Crafton, J., A. Forlines, S. Palluconi, K.-Y. Hsu, C. Carter, and M. Gruber (2011), Investigation of transverse jet injections in a supersonic crossflow using fast responding pressure-sensitive paint, *AIAA Paper 2011-3522*, American Institute of Aeronautics and Astronautics, Reston, Va.

Crist, S., P. M. Sherman, and D. R. Glass (1966), Study of the highly underexpanded sonic jet, *AIAA J.*, *4*, 68–71.

Donaldson, C. D., and R. S. Snedeker (1971), Study of free jet impingement. 1: Mean properties of free and impinging jets, *J. Fluid Mech.*, *45*, 281–319.

Donnadieu, F., and O. Merle (2001), Geometrical constraints of the 1980 Mount St. Helens intrusion from analogue models, *Geophys. Res. Lett.*, *28*, 639–642.

Esposti Ongaro, T., C. Cavazzoni, G. Erbacci, A. Neri, and M. V. Salvetti (2007), A parallel multiphase flow code for the 3D simulation of explosive volcanic eruptions, *Parallel Comput.*, *33*, 541–560.

Esposti Ongaro, T., A. B. Clarke, A. Neri, B. Voight, and C. Widiwijayanti (2008), Fluid dynamics of the 1997 Boxing Day volcanic blast on Montserrat, West Indies, *J. Geophys. Res.*, *113*, B03211, doi:10.1029/2006JB004898.

Esposti Ongaro, T., C. Widiwijayanti, A. B. Clarke, B. Voight, and A. Neri (2011), Multiphase-flow numerical modeling of the 18 May 1980 lateral blast at Mount St. Helens USA, *Geology*, *39*, 535–538.

Esposti Ongaro, T., A. B. Clarke, B. Voight, A. Neri, and C. Widiwijayanti (2012), Multiphase flow dynamics of pyroclastic density currents during the May 18, 1980 lateral blast of Mount St. Helens, *J. Geophys. Res.*, *117*, B06208, doi:10.1029/2011JB009081.

Flaherty, W., T. M. Reedy, G. S. Elliott, J. M. Austin, R. Schmit, and J. Crafton (2014), Investigation of cavity flow using fast-response pressure sensitive paint, *AIAA J.*, doi:10.2514/1.J052864, in press.

Fonov, S., G. Jones, J. Crafton, V. Fonov, and L. Goss (2006), The development of optical techniques for the measurement of pressure and skin friction, *Meas. Sci. Technol.*, *17*(6), 1261–1268.

Hoblitt, R. P. (2000), Was the 18 May 1980 lateral blast at Mt. St. Helens the product of two explosions?, *Philos. Trans. R. Soc. London, Ser. A*, *358*, 1639–1661.

Ivanov, M. Y., and V. P. Nazarov (1974), "Lateral" interaction of a supersonic underexpanded ideal-gas jet with surfaces of different shape, *Fluid Dyn.*, *9*, 867–871, Translated from Izvestiya Akademii Nauk SSSR, Mekhanika Zhidkosti i Gaza No. 6, pp. 3–8.

Khalil, I., and D. R. Miller (2004), The structure of supercritical fluid free-jet expansions, *AIChE J.*, *50*, 2697–2704.

Kieffer, S. W. (1981), Blast dynamics at Mount St. Helens on 18 May 1980, *Nature*, *291*, 568–570.

Kieffer, S. W. (1982), Fluid dynamics of the May 18 blast at Mount St. Helens, in *The 1980 Eruptions of Mount St. Helens*, edited by P. W. Lipman and D. R. Mullineaux, pp. 379–400, U. S. Geol. Survey Prof. Paper 1250, Washington, D. C.

Kieffer, S. W., and B. Sturtevant (1984), Laboratory studies of volcanic jets, *J. Geophys. Res.*, *89*, 8253–8268.

Lamont, P. J., and B. L. Hunt (1980), The impingement of underexpanded, axisymmetric jets on perpendicular and inclined flat plates, *J. Fluid Mech.*, *100*, 471–511.

Lengrand, J.-C., J. Allegre, and M. Raffin (1982), Underexpanded free jets and their interaction with adjacent surfaces, *AIAA J.*, *20*, 27–28.

Liepmann, H. W., and A. Roshko (2001), *Elements of Gasdynamics*, Dover Publications, New York.

Mark, H. (1958), The interaction of a reflected shock wave with the boundary layer in a shock tube, *Tech. Rep. 1418*, National Aeronautics and Space Administration.

Moore, J. G., and C. J. Rice (1984), *Explosive Volcanism: Inception, Evolution, and Hazards, Studies in Geophysics,* chap. 10, pp. 133–142, National Academy Press, Washington, D. C.

Nakai, Y., N. Fujimatsu, and K. Fujii (2006), Experimental study of underexpanded supersonic jet impingement on an inclined flat plate, *AIAA J.*, *44*, 2691–2699.

Ogden, D., K. H. Wohletz, G. Glatzmaier, and E. E. Brodsky (2008a), Numerical simulation of volcanic jets: Importance of vent overpressure, *J. Geophys. Res.*, *113*, B02204, doi:10.1029/2007JB005133.

Ogden, D. (2011), Fluid dynamics in explosive volcanic vents and craters, *Earth Planet. Sci. Lett.*, *312*, 401–410.

Ogden, D. E., G. A. Glatzmaier, and K. H. Wohletz (2008b), Effects of vent overpressure on buoyant eruption columns: Implications for plume stability, *Earth Planet. Sci. Lett.*, *268*(3-4), 283–292, doi:10.1016/j.epsl.2008.01.014.

Orescanin, M. M., and J. M. Austin (2010), Exhaust of underexpanded jets from finite reservoirs, *J. Propul. Power*, *26*(4), 744–753.

Orescanin, M. M., J. M. Austin, and S. W. Kieffer (2010), Unsteady high-pressure flow experiments with applications to explosive volcanic eruptions, *J. Geophys. Res.*, *115*, B06206, doi:10.1029/2009JB006985.

Plemmons, D. H., M. Mehta, B. C. Clark, S. P. Kounaves, L. L. Peach Jr., N. O. Renno, L. Tamppari, and S. M. M. Young (2008), Effects of the Phoenix Lander descent thruster plume on the Martian surface, *J. Geophys. Res.*, *113*, E00A11, doi:10.1029/2007JE003059.

Valentine, G. A., K. H. Wohletz, and S. W. Kieffer (1992), Effects of topography on facies and compositional zonation in caldera-related ignimbrites, *Geol. Soc. Am. Bull.*, *104*, 154–165.

Wlezien, R. W. (1989), Near-field acoustic environment of a supersonic plume adjacent to a wall, *AIAA PAPER 89-1137*, McDonnell Douglas Research Laboratories, Saint Louis, Mo.

Wu, J. X., L. Tang, E. A. Luke, X.-L. Tong, and P. Cinnella (2002), Comprehensive numerical study of jet-flow impingement over flat plates, *J. Spacecraft Rockets*, *39*, 357–366.